B_6 ring building blocks

DOI: 10.1002/anie.201309469

Hexagonal Bipyramidal $[Ta_2B_6]^{-/0}$ Clusters: B_6 Rings as Structural Motifs**

Wei-Li Li, Lu Xie, Tian Jian, Constantin Romanescu, Xin Huang, and Lai-Sheng Wang**

Abstract: *It has been a long-sought goal in cluster science to discover stable atomic clusters as building blocks for cluster-assembled nanomaterials, as exemplified by the fullerenes and their subsequent bulk syntheses.[1,2] Clusters have also been considered as models to understand bulk properties, providing a bridge between molecular and solid-state chemistry.[3] Because of its electron deficiency, boron is an interesting element with unusual polymorphism. While bulk boron is known to be dominated by the three-dimensional (3D) B_{12} icosahedral motifs,[4] new forms of elemental boron are continuing to be discovered.[5] In contrast to the 3D cages commonly found in bulk boron, in the gas phase two-dimensional (2D) boron clusters are prevalent.[6–8] The unusual planar boron clusters have been suggested as potential new bulking blocks or ligands in chemistry.[6a] Herein we report a joint experimental and theoretical study on the $[Ta_2B_6]^-$ and $[Ta_2B_6]$ clusters. We found that the most stable structures of both the neutral and anion are D_{6h} bipyramidal, similar to the recently discovered MB_6M structural motif in the $Ti_7Rh_4Ir_2B_8$ solid compound.[9]*

Metal-boron clusters, $[LiB_6]^-$ and $[LiB_8]^-$, were previously observed and investigated using photoelectron spectroscopy (PES) and ab initio calculation.[10,11] In these clusters, the lithium atom was found to form charge-transfer complexes, $Li^+[B_6^{2-}]$ or $Li^+[B_8^{2-}]$, in which the geometries or electronic structures of the boron clusters[6b,c] were not changed significantly. The NaB_3 cluster was also calculated to be a C_{3v} $Na^+[B_3^-]$ ionic species.[12] Complexes of the planar B_5 and B_6 clusters with alkali ($M^+B_5^-$) and alkali-earth ($M^{2+}B_6^-$) elements were calculated, where the B_5 and B_6 units were found to similar to the bare clusters, respectively.[13]

The first synthesized and structurally characterized compounds containing planar boron clusters as ligands were the triple-decker $[(Cp^*Re)_2B_nX_n]$ ($n = 5$, 6; X = H or Cl, $Cp^* = Me_5C_5$), in which the B_nX_n unit was found to be perfectly planar pentagonal or hexagonal motif.[14,15] The electronic structures of these two complexes are interesting, where the Re atoms can be viewed to donate six electrons to the planar B_nX_n units as hexa-charged species.[14] Similar hexa-charged $[B_5H_5]^{6-}$ and $[B_6H_6]^{6-}$ units have been predicted theoretically in $Li_6B_5H_5$ and $Li_6B_6H_6$.[16] A number of planar cyclic B_5- or B_6- containing compounds have been synthesized with either different metal atoms or different ligands.[17]

However, all the planar boron rings in the above mentioned compounds were actually B_5X_5 or B_6X_6 species.[14–17] The only bare planar B_6 ring as a structural motif was discovered recently in the solid compound $Ti_7Rh_4Ir_2B_8$,[9] in which the B_6 ring is sandwiched between two metal atoms in a bipyramidal fashion. Boron is also known to form graphene-like structures in MgB_2,[18] in which the B atom can be viewed as B^- (iso-electronic to C). In single transition-metal-doped boron clusters ($[MB_n]^-$), the transition-metal atom has been found to prefer occupying the central position of a boron ring to form molecular wheels with octa-, hepta-, and deca-coordination numbers, depending on the nature and oxidation states of the dopants.[19–23] A series of $[TaB_n]^-$ ($n = 3$–9) clusters has been recently studied and the B atoms were found to nucleate around the Ta atom leading up to the decacoordinate $[Ta©B_{10}]^-$ molecular wheel (the © sign is used to designate the central position of the doped atom in monocyclic structures in $[M©B_n]$-type planar clusters).[24] A computational study of $[FeB_n]$ ($n = 1$–10) was reported with both 2D and 3D structures.[25]

Di-metal doped boron clusters ($[M_2B_n]$) are relatively unexplored in comparison to the mono-metal doped boron clusters. Calculations of $[Li_2B]^-$ and $[Au_2B_2]^-$ were reported.[26,27] A joint PES and theoretical study found that two Au atoms covalently bond to the planar B_7 in the $[Au_2B_7]^-$ cluster,[28] similar to the structural pattern of $[H_2B_7]^-$.[29,30] Very recently, a combined experimental and theoretical study on di-tantalum doped boron clusters ($[Ta_2B_n]^-$) were carried out, showing that boron atoms build around a Ta–Ta dimer equatorially from $[Ta_2B_2]^-$ to $[Ta_2B_5]^-$,[31] in which strong Ta–Ta bonding still exists. Herein, the $[Ta_2B_6]^-$ cluster is investigated. Both $[Ta_2B_6]^-$ and $[Ta_2B_6]$ are found to be bipyramidal with a B_6 ring sandwiched by the two Ta atoms.

The $[Ta_2B_6]^-$ cluster was produced in a laser vaporization supersonic cluster beam source (see the Experimental

[*] W. L. Li, T. Jian, Dr. C. Romanescu, Prof. Dr. L.-S. Wang
Department of Chemistry, Brown University
Providence, RI 02912 (USA)
E-mail: Lai-Sheng_Wang@brown.edu
Homepage: http://casey.brown.edu/chemistry/research/LSWang/index.html
L. Xie, Prof. Dr. X. Huang
Department of Chemistry
Fuzhou University
Fuzhou, Fujian 350108 (China)
E-mail: xhuang@fzu.edu.cn
Prof. Dr. X. Huang
Fujian Provincial Key Laboratory of Theoretical and Computational Chemistry, Xiamen, Fujian 361005 (China)

[**] This work is supported by the National Science Foundation (CHE-1263745 to L.S.W.) and the National Natural Science Foundation of China (21071031 and 21371034 to X. H.), the Natural Science Foundation of Fujian Province for Distinguished Young Investigator Grant (2013J06004 to X.H.).

Supporting information for this article is available on the WWW under http://dx.doi.org/10.1002/anie.201309469.

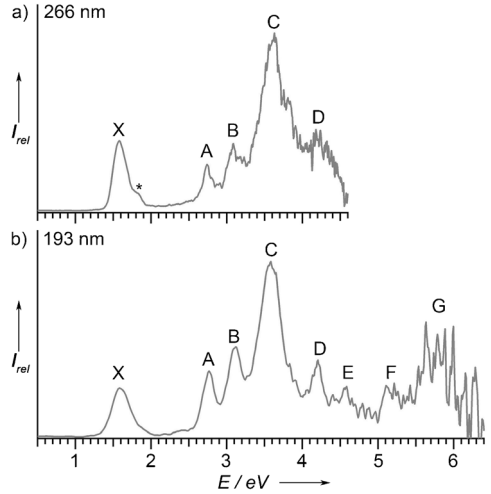

Figure 1. Photoelectron spectra of $[Ta_2B_6]^-$ at 266 and 193 nm plotted in electron binding energies. See text and Table 1 for details.

Table 1: Experimental vertical detachment energies (VDE) and calculations using ΔSCF-TDDFT for $[Ta_2B_6]^-$.

Band	VDE (exp)[a]	Final States and Electronic Configuration	BP86[b]
X	1.59(3)	$^1A_{1g}$ ... $1e_{2g}^4 1a_{2u}^2 2a_{1g}^2 1b_{2u}^2 1e_{1g}^4 2e_{1u}^4 1e_{2u}^4 3a_{1g}^0$	1.67
A	2.74(5)	$^3E_{2u}$ ... $1e_{2g}^4 1a_{2u}^2 2a_{1g}^2 1b_{2u}^2 1e_{1g}^4 2e_{1u}^4 1e_{2u}^3 3a_{1g}^1$	2.77
B	3.08(5)	$^1E_{2u}$ ... $1e_{2g}^4 1a_{2u}^2 2a_{1g}^2 1b_{2u}^2 1e_{1g}^4 2e_{1u}^4 1e_{2u}^3 3a_{1g}^1$	2.97
C	3.61(5)	$^3E_{1u}$ ... $1e_{2g}^4 1a_{2u}^2 2a_{1g}^2 1b_{2u}^2 1e_{1g}^4 2e_{1u}^3 1e_{2u}^4 3a_{1g}^1$	3.37
		$^1E_{1u}$ ... $1e_{2g}^4 1a_{2u}^2 2a_{1g}^2 1b_{2u}^2 1e_{1g}^4 2e_{1u}^3 1e_{2u}^4 3a_{1g}^1$	3.66
D	4.21(5)	$^3E_{1g}$ ... $1e_{2g}^4 1a_{2u}^2 2a_{1g}^2 1b_{2u}^2 1e_{1g}^3 2e_{1u}^4 1e_{2u}^4 3a_{1g}^1$	4.18
E	4.57(5)	$^1E_{1g}$ ... $1e_{2g}^4 1a_{2u}^2 2a_{1g}^2 1b_{2u}^2 1e_{1g}^3 2e_{1u}^4 1e_{2u}^4 3a_{1g}^1$	4.26
F	5.11(5)	$^3B_{2u}$ ... $1e_{2g}^4 1a_{2u}^2 2a_{1g}^2 1b_{2u}^1 1e_{1g}^4 2e_{1u}^4 1e_{2u}^4 3a_{1g}^1$	4.90
		$^1B_{2u}$ ... $1e_{2g}^4 1a_{2u}^2 2a_{1g}^2 1b_{2u}^1 1e_{1g}^4 2e_{1u}^4 1e_{2u}^4 3a_{1g}^1$	4.99
G	ca. 5.8	$^3A_{1g}$ ... $1e_{2g}^4 1a_{2u}^2 2a_{1g}^1 1b_{2u}^2 1e_{1g}^4 2e_{1u}^4 1e_{2u}^4 3a_{1g}^1$	5.69
		$^1A_{1g}$ ... $1e_{2g}^4 1a_{2u}^2 2a_{1g}^1 1b_{2u}^2 1e_{1g}^4 2e_{1u}^4 1e_{2u}^4 3a_{1g}^1$	5.80
		$^3A_{2u}$ ... $1e_{2g}^4 1a_{2u}^1 2a_{1g}^2 1b_{2u}^2 1e_{1g}^4 2e_{1u}^4 1e_{2u}^4 3a_{1g}^1$	6.04
		$^1A_{2u}$ ... $1e_{2g}^4 1a_{2u}^1 2a_{1g}^2 1b_{2u}^2 1e_{1g}^4 2e_{1u}^4 1e_{2u}^4 3a_{1g}^1$	6.14

[a] Numbers in the parentheses are the uncertainty in the last digit. [b] The VDEs were calculated at BP86/Ta/Stuttgart + 2f1g/B/aug-cc-pVTZ level of theory.

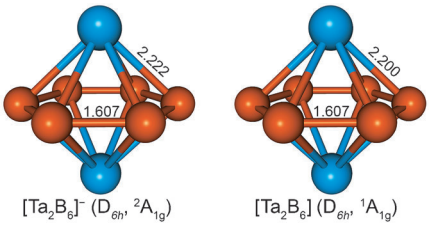

Figure 2. Optimized structures of $[Ta_2B_6]^-$ and $[Ta_2B_6]$ at the BP86/Ta/Stuttgart + 2f1g/B/aug-cc-pVTZ level of theory. Bond lengths in [Å]. Ta blue, B orange.

Section). The photoelectron spectra of $[Ta_2B_6]^-$ are shown in Figure 1 at two photon energies. We also measured the spectra at 532 and 355 nm (Figure S1 in supporting information), which give better resolved data for the lowest binding energy band (X). The first vertical detachment energy (VDE) of 1.58 eV is obtained from the 532 nm spectrum. Since no clear vibrational progression was resolved for band X, the adiabatic detachment energy (ADE) was evaluated by drawing a straight line along the leading edge of the X band in the 532 nm spectrum and then adding the experimental resolution to the intersection with the binding energy axis. The ADE so measured is 1.51 ± 0.03 eV, which also represents the electron affinity of neutral $[Ta_2B_6]$. The next major detachment band, labeled as A in Figure 1, has a VDE of 2.74 eV. The energy separation of 1.15 eV between bands X and A represents a large gap between the highest occupied (HOMO) and lowest unoccupied (LUMO) molecular orbitals of $[Ta_2B_6]$, indicating its high electronic stability with a closed-shell electron configuration. Three more well-resolved bands (B, C, and D) are observed in the 266 nm spectrum (Figure 1 a). The intense band C at 3.61 eV is quite broad and it may contain multiple detachment transitions. More detachment transitions were observed in the 193 nm spectrum (Figure 1 b), band E at a VDE of 4.57 eV and band F at 5.11 eV. There are more congested features at higher binding energies beyond 5.5 eV, where the signal-to-noise ratios were poor. The label G is only for the sake of discussion. All the VDEs are summarized in Table 1, where they are compared with the calculated VDEs of the global minimum of $[Ta_2B_6]^-$.

The weak signal labeled as "*" at 1.88 eV in Figure 1 a is probably due to contributions of a low-lying isomer. This feature is resolved into a well-defined peak in the 355 nm spectrum (Figure S1b). Weak signals were also present at approximately 2.5 eV as a tail to the A band. These signals seemed to be enhanced in the 355 nm spectrum and may have the common origin as the 1.88 eV feature.

Global minimum searches for $[Ta_2B_6]^-$ and $[Ta_2B_6]$ were performed using the density functional theory (DFT) with analytical gradients. Candidate structures with a variety of initial geometries and spin multiplicities were taken into consideration (see the Experimental Section). The D_{6h}-bipyramid structure ($^2A_{1g}$; Figure 2) with a B_6 ring turned out to be the global minimum for $[Ta_2B_6]^-$. The B–B bond length is 1.607 Å and the Ta–B bond length is 2.222 Å. The neutral $[Ta_2B_6]$ was found to have a very similar D_{6h} bipyramidal structure ($^1A_{1g}$) with the same B–B bond length as that in the anion except that the Ta–B distance is shortened by about 0.02 Å. The nearly identical structures of the anion and neutral suggest the first electron detachment is likely from a non-bonding orbital, confirming the electronic and structural stability of $[Ta_2B_6]$. The similar structures of the anion and neutral species are also consistent with the sharp ground-state PES band (X). All the other low-lying isomers of $[Ta_2B_6]^-$ and $[Ta_2B_6]$ are presented in Figure S2 and S3, respectively.

To further confirm the bipyramidal global minimum structure for $[Ta_2B_6]^-$, we computed the VDEs at BP86[32]/Ta/Stuttgart + 2f1g[33]/B/aug-cc-pVTZ,[34] which was found previously to give superior results for energetic properties for clusters involving early transition metals.[35] The calculated VDEs are compared with the experimental data in Table 1. The first VDE corresponds to electron detachment from the $3a_{1g}$ HOMO to yield the $^1A_{1g}$ neutral ground state. The calculated VDE of 1.67 eV agrees well with the experimental value of 1.59 eV. The calculated ADE of 1.63 eV is also in

good agreement with the experimental ADE of 1.51 eV. The next detachment channel is from the $1e_{2u}$ HOMO−1 to produce a $^3E_{2u}$ final state. The calculated VDE of 2.77 eV is in excellent agreement with the VDE of the A band at 2.74 eV. The calculated VDE for the corresponding singlet state is 2.97 eV, which is assigned to the observed PES band B at 3.08 eV. The calculated higher binding energy detachment channels are all in good agreement with the experimental observations (Table 1). Indeed, a number of detachment channels contribute to the congested features above 5.5 eV (bands G). The excellent overall agreement between the calculated VDEs and the experimental data lends considerable credence to the D_{6h} global minimum found for $[Ta_2B_6]^-$.

The second low-lying isomer (D_{6h}, $^2A_{2u}$) of $[Ta_2B_6]^-$ (Figure S2) is 0.19 eV and 0.31 eV above the global minimum at the BP86 and CCSD(T)[36] levels of theory, respectively. The structure of this isomer is similar to the global minimum, corresponding to electron occupation of the LUMO + 1 of the D_{6h} neutral $[Ta_2B_6]$. Its calculated VDEs are given in Table S1. Its first calculated VDE of 1.46 eV is lower than that of the global minimum by about 0.2 eV. The lower binding-energy side of band X in the experimental spectra (Figure 1 and Figure S1) was pretty clean, indicating that the population of this isomer in our experiment was negligible. The next low-lying isomer at the CCSD(T) level is 0.76 eV above the global minimum. This isomer has a quartet electronic state ($^4A_{2u}$) with D_{2h} symmetry. Even though it is energetically unfavorable, it might be a long-lived state because the relaxation to the ground state is spin-forbidden. Its computed VDEs are given in Table S2. Interestingly, its first VDE is calculated to be 1.94 eV, in good agreement with the "*" feature at 1.88 eV (Figure 1). Its second VDE was calculated to be 2.18 eV, consistent with the low-binding-energy tail off band A. Thus, we conclude that this isomer was weakly populated in our experiment and it might also contribute to the congestion of the higher binding energy side of the observed spectra. Such "spin-protected" high-lying isomers have been observed in a number of clusters previously.[6d,37]

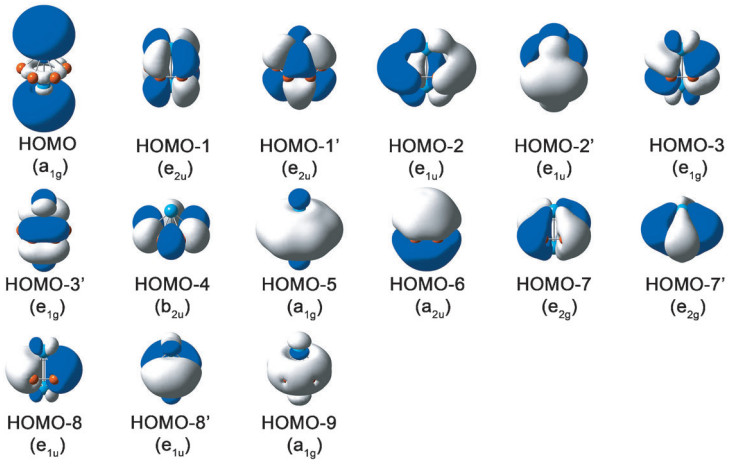

Figure 3. Valence conical orbitals of $[Ta_2B_6]^-$ at the BP86/Ta/Stuttgart + 2f1g/B/aug-cc-pVTZ level of theory.

Figure 3 displays the valence conical MOs for the global minimum of $[Ta_2B_6]^-$. The orbital energies are shown in Figure S4. The HOMO (a_{1g}) is a non-bonding orbital composed mainly of the Ta 6s and 6p atomic orbitals. Electron detachment from this orbital is not expected to change the symmetry or structure of the resulting neutral cluster much, in agreement with the nearly identical structures of the D_{6h} $[Ta_2B_6]^-$ and $[Ta_2B_6]$ and the sharp ground state PES band (X). The HOMO−1 (e_{2u}) is doubly degenerate, consisting mainly of two Ta 5d δ-type orbitals with antibonding characters. The HOMO−2 (e_{1u}) and HOMO−5 (a_{1g}) are three σ-type orbitals delocalized mainly over the B_6 ring, whereas the HOMO−3 (e_{1g}) and HOMO−6 (a_{2u}) are three π type orbitals delocalized over the B_6 ring. All these six boron-based orbitals interact with the Ta 5d orbitals along the Ta–Ta axis.

We analyzed the chemical bonding of the closed-shell D_{6h} $[Ta_2B_6]$ using the adaptive natural density partitioning (AdNDP) method,[38] which localizes the computed density matrix into *n*-center two-electron (*n*c-2e) bonds, with *n* ranging from one to the total number of atoms in the molecule. The AdNDP analyses (Figure 4) provide a relatively simple

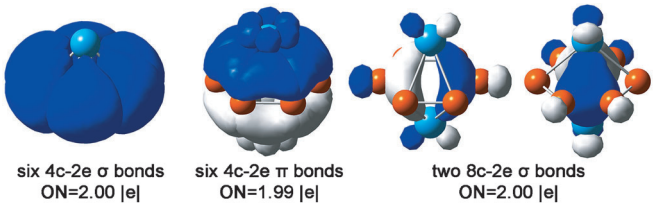

Figure 4. Chemical bonding analyses of $[Ta_2B_6]$ using the AdNDP method. ON stands for occupation number.

bonding picture for the Ta-B_6-Ta inverse-sandwich structure. There are six 4c-2e σ-type bonds, each of which involves one B–B bond and the two Ta atoms. These six bonds are essentially the six B–B bonds, forming the B_6 ring. The interactions between the B_6 ring and the apex Ta atoms are through the six 4c-2e π bonds and, interestingly, two totally delocalized 8c-2c bonds. Hence, the AdNDP analyses reveal that all 28 valence electrons in $[Ta_2B_6]$ are participating in the chemical bonding, underlying the electronic and geometrical stability of the bipyramidal $[Ta_2B_6]$. The chemical bonding analysis shows that there is no significant direct Ta–Ta interaction, consistent with the relatively long Ta–Ta distance (3.01 Å) in $[Ta_2B_6]$. Interestingly, in $[(Cp^*Re)_2B_6H_4Cl_2]$, the Re–Re distance is much shorter (2.689 Å),[14] indicating significant Re–Re bonding, probably due to the larger B_6 ring in the $B_6H_4Cl_2$ moiety.

In conclusion, we report the first gas-phase cluster containing a planar B_6 ring coordinated by two Ta atoms in a bipyramidal structure. Photoelectron spectroscopy revealed that neutral $[Ta_2B_6]$ is an electronically highly stable system with a closed-shell electron configuration and a large HOMO–

LUMO gap. Global minimum searches found a bipyramidal $[Ta_2B_6]$ to be the most stable structure. AdNDP analyses revealed the nature of the B_6 and Ta interactions and uncovered strong covalent bonding between B_6 and Ta. The D_{6h}-$[TaB_6Ta]$ gaseous cluster is reminiscent of the structural pattern in the ReB_6X_6Re core in the $[(Cp^*Re)_2B_6H_4Cl_2]$[14] and the TiB_6Ti motif in the newly synthesized $Ti_7Rh_4Ir_2B_8$ solid-state compound.[9] The current work provides an intrinsic link between a gaseous cluster and motifs for solid materials. Continued investigations of the transition-metal boron clusters may lead to the discovery of new structural motifs involving pure boron clusters for the design of novel boride materials.

Experimental Section

Photoelectron spectroscopy: The experiment was carried out using a magnetic-bottle PES apparatus equipped with a laser vaporization cluster source, details of which have been published elsewhere.[39] Briefly, the $[Ta_2B_6]^-$ cluster was generated by laser ablation of a cold-pressed target composed of Ta, isotopically enriched ^{11}B, and Ag or Bi. The Ag or Bi was added as binders for the preparation of the target and also provided convenient calibrants (Ag^- or Bi^-) for the PES. Clusters formed in the source were entrained by a He carrier gas and underwent a supersonic expansion to form a collimated cluster beam. The He carrier gas was seeded with 5% Ar to achieve better supersonic cooling.[40] The anionic clusters were extracted from the cluster beam and analyzed in a time-of-fight mass spectrometer. The $[Ta_2B_6]^-$ clusters of interest were mass-selected and decelerated before being photodetached by a laser beam operated at 193 nm (6.424 eV), 266 nm (4.661 eV), 355 nm (3.496 eV), or 532 nm (2.331 eV). Photoelectrons were collected at nearly 100% efficiency by a magnetic bottle and analyzed in a 3.5 m long electron flight tube. The resolution of the apparatus, $\Delta E_k/E_k$, was better than 2.5%, that is, ca. 25 meV for 1 eV electrons.

Theoretical calculations: The DFT calculations were carried out at the BP86 level.[32] Numerous structural candidates with different initial structures and spin states were investigated and global minimum searches were performed using analytical gradients with the Stuttgart relativistic small core basis set and an effective core potential[41] augmented with two f-type and one g-type polarization functions for Ta [$\zeta(f) = 0.210, 0.697$; $\zeta(g) = 0.472$] as recommended by Martin and Sundermann[33] and the aug-cc-pVTZ basis set for boron.[34] Scalar relativistic effects, namely, the mass velocity and Darwin effects, were taken into account by the quasi-relativistic pseudopotentials. Vibrational-frequency calculations were done to verify the nature of the stationary points. The low-lying isomers revealed by the searches were further evaluated by single-point calculations at the coupled cluster CCSD(T) level[36] with the Ta/Stuttgart + 2f1g/B/aug-cc-pVTZ basis sets at the BP86 geometries. For open-shell systems, the R/UCCSD(T) approach was used, where a restricted open-shell Hartree–Fock (ROHF) calculation was initially performed and the spin constraint was relaxed in the correlation treatment. In addition, further accurate optimizations in CCSD(T) were carried out for the first four low-lying structures with the Ta/Stuttgart + 2f1g/B/aug-cc-pVTZ basis sets. All DFT calculations were done with the Gaussian 03 software package,[42] and the coupled-cluster calculations were performed using the MOLPRO 2010.1 package.[43] Molecular structures of $[Ta_2B_6]^-$ and $[Ta_2B_6]$ are plotted using Molekel 5.4.0.8.[44] Three-dimensional contours of the molecular orbitals (MOs) were visualized using the GaussView 4.1.2.[45] Different exchange-correlation functionals were tested for accuracy and consistency.

Vertical detachment energies (VDEs) were calculated using a combined ΔSCF-TDDFT approach. In this approach, the ground-state energies of the anions and the neutrals were calculated from the ΔSCF energy difference at the BP86 level, whereas the excited states of the one-electron-detached species were obtained from TDDFT calculations of the neutrals.[46] The BP86 functional showed superior results in terms of electron binding energies and structures for the $[Ta_2B_6]^-$ cluster. Therefore, we used the results with the BP86 functional for our direct comparison with the experiment. Chemical bonding analyses of $[Ta_2B_6]$ were performed using the AdNDP method.[38] GaussView 4.1.2 was used for the bond visualization.[45]

Received: October 31, 2013
Published online: December 18, 2013

Keywords: ab initio calculations · B_6 ring · boron clusters · photoelectron spectroscopy · tantalum

[1] H. W. Kroto, J. R. Heath, S. C. O'Brien, R. F. Curl, R. E. Smalley, *Nature* **1985**, *318*, 162 – 163.
[2] W. Krätschmer, L. D. Lamb, K. Fostiropoulos, D. R. Huffman, *Nature* **1990**, *347*, 354 – 358.
[3] T. P. Fehlner, J.-F. Halet, J.-Y. Saillard, *Molecular Clusters: A Bridge to Solid-State Chemitry*, Cambridge University Press, UK, **2007**.
[4] a) N. Vast, S. Baroni, G. Zerah, J. M. Besson, A. Polian, M. Grimsditch, J. C. Chervin, *Phys. Rev. Lett.* **1997**, *78*, 693 – 696; b) M. Fujimori, T. Nakata, T. Nakayama, E. Nishibori, K. Kimura, M. Takata, M. Sakata, *Phys. Rev. Lett.* **1999**, *82*, 4452 – 4455.
[5] B. Albert, H. Hillebrecht, *Angew. Chem.* **2009**, *121*, 8794 – 8824; *Angew. Chem. Int. Ed.* **2009**, *48*, 8640 – 8668.
[6] a) A. N. Alexandrova, A. I. Boldyrev, H. J. Zhai, L. S. Wang, *Coord. Chem. Rev.* **2006**, *250*, 2811 – 2866; b) A. N. Alexandrova, A. I. Boldyrev, H. J. Zhai, L. S. Wang, E. Steiner, P. W. Fowler, *J. Phys. Chem. A* **2003**, *107*, 1359 – 1369; c) H. J. Zhai, A. N. Alexandrova, K. A. Birch, A. I. Boldyrev, L. S. Wang, *Angew. Chem.* **2003**, *115*, 6186 – 6190; *Angew. Chem. Int. Ed.* **2003**, *42*, 6004 – 6008; d) H. J. Zhai, B. Kiran, J. Li, L. S. Wang, *Nat. Mater.* **2003**, *2*, 827 – 833; e) W. Huang, A. P. Sergeeva, H. J. Zhai, B. B. Averkiev, L. S. Wang, A. I. Boldyrev, *Nat. Chem.* **2010**, *2*, 202 – 206; f) I. A. Popov, Z. A. Piazza, W. L. Li, L. S. Wang, A. I. Boldyrev, *J. Chem. Phys.* **2013**, *139*, 144307.
[7] a) B. Kiran, S. Bulusu, H. J. Zhai, S. Yoo, X. C. Zeng, L. S. Wang, *Proc. Natl. Acad. Sci. USA* **2005**, *102*, 961 – 964; b) T. B. Tai, N. M. Tam, M. T. Nguyen, *Chem. Phys. Lett.* **2012**, *530*, 71 – 76.
[8] E. Oger, N. R. M. Crawford, R. Kelting, P. Weis, M. M. Kappes, R. Ahlrichs, *Angew. Chem.* **2007**, *119*, 8656 – 8659; *Angew. Chem. Int. Ed.* **2007**, *46*, 8503 – 8506.
[9] B. P. T. Fokwa, M. Hermus, *Angew. Chem.* **2012**, *124*, 1734 – 1737; *Angew. Chem. Int. Ed.* **2012**, *51*, 1702 – 1705.
[10] A. N. Alexandrova, A. I. Boldyrev, H. J. Zhai, L. S. Wang, *J. Chem. Phys.* **2005**, *122*, 054313.
[11] A. N. Alexandrova, H. J. Zhai, L. S. Wang, A. I. Boldyrev, *Inorg. Chem.* **2004**, *43*, 3552 – 3554.
[12] A. Kuznetsov, A. Boldyrev, *Struct. Chem.* **2002**, *13*, 141 – 148.
[13] a) Q. S. Li, Q. Jin, *J. Phys. Chem. A* **2004**, *108*, 855 – 860; b) Q. S. Li, Q. Jin, *J. Phys. Chem. A* **2003**, *107*, 7869 – 7873.
[14] B. Le Guennic, H. Jiao, S. Kahlal, J.-Y. Saillard, J.-F. Halet, S. Ghosh, M. Shang, A. M. Beatty, A. L. Rheingold, T. P. Fehlner, *J. Am. Chem. Soc.* **2004**, *126*, 3203 – 3217.
[15] S. Ghosh, A. M. Beatty, T. P. Fehlner, *J. Am. Chem. Soc.* **2001**, *123*, 9188 – 9189.
[16] a) A. N. Alexandrova, K. A. Birch, A. I. Boldyrev, *J. Am. Chem. Soc.* **2003**, *125*, 10786 – 10787; b) A. N. Alexandrova, A. I. Boldyrev, *Inorg. Chem.* **2004**, *43*, 3588 – 3592.
[17] a) A. Lupan, R. B. King, *Polyhedron* **2013**, *32*, 151 – 157; b) T. P. Fehlner, *J. Organomet. Chem.* **2009**, *694*, 1671 – 1677; c) S. K.

Bose, S. Ghosh, B. C. Noll, J.-F. Halet, J.-Y. Saillard, A. Vega, *Organometallics* **2007**, *26*, 5377 – 5385; d) S. K. Bose, K. Geetharani, B. Varghese, S. M. Mobin, S. Ghosh, *Chem. Eur. J.* **2008**, *14*, 9058 – 9064; e) R. S. Dhayal, K. K. V. Chakrahari, V. Ramkumar, S. Ghosh, *J. Cluster Sci.* **2009**, *20*, 565 – 572; f) K. Geetharani, S. K. Bose, G. Pramanik, T. K. Saha, V. Ramkumar, S. Ghosh, *Eur. J. Inorg. Chem.* **2009**, 1483 – 1487; g) S. Sahoo, K. H. K. Reddy, R. S. Dhayal, S. M. Mobin, V. Ramkumar, E. D. Jemmis, S. Ghosh, *Inorg. Chem.* **2009**, *48*, 6509 – 6516; h) R. S. Dhayal, K. K. V. Chakrahari, B. Varghese, S. M. Mobin, S. Ghosh, *Inorg. Chem.* **2010**, *49*, 7741 – 7747; i) S. K. Bose, K. Geetharani, S. Ghosh, *Chem. Commun.* **2011**, *47*, 11996 – 11998; j) K. Geetharani, B. S. Krishnamoorthy, S. Kahlal, S. M. Mobin, J.-F. Halet, S. Ghosh, *Inorg. Chem.* **2012**, *51*, 10176 – 10184; k) B. S. Krishnamoorthy, S. Kahlal, B. Le Guennic, J.-Y. Saillard, S. Ghosh, J.-F. Halet, *Solid State Sci.* **2012**, *14*, 1617 – 1623; l) A. Lupan, R. B. King, *Inorg. Chem.* **2012**, *51*, 7609 – 7616.

[18] a) J. Nagamatsu, N. Nakagawa, T. Muranaka, Y. Zenitani, J. Akimitsu, *Nature* **2001**, *410*, 63 – 64; b) M. Monteverde, M. Núñez-Regueiro, N. Rogado, K. A. Regan, M. A. Hayward, T. He, S. M. Loureiro, R. J. Cava, *Science* **2001**, *292*, 75 – 77.

[19] C. Romanescu, T. R. Galeev, W. L. Li, A. I. Boldyrev, L. S. Wang, *Angew. Chem.* **2011**, *123*, 9506 – 9509; *Angew. Chem. Int. Ed.* **2011**, *50*, 9334 – 9337.

[20] T. R. Galeev, C. Romanescu, W. L. Li, L. S. Wang, A. I. Boldyrev, *Angew. Chem.* **2012**, *124*, 2143 – 2147; *Angew. Chem. Int. Ed.* **2012**, *51*, 2101 – 2105.

[21] W. L. Li, C. Romanescu, T. R. Galeev, Z. A. Piazza, A. I. Boldyrev, L. S. Wang, *J. Am. Chem. Soc.* **2012**, *134*, 165 – 168.

[22] C. Romanescu, T. R. Galeev, A. P. Sergeeva, W. L. Li, L. S. Wang, A. I. Boldyrev, *J. Organomet. Chem.* **2012**, *697-697*, 148 – 154.

[23] C. Romanescu, T. R. Galeev, W. L. Li, A. I. Boldyrev, L. S. Wang, *Acc. Chem. Res.* **2013**, *46*, 350 – 358.

[24] W. L. Li, A. S. Ivanov, J. Federic, C. Romanescu, I. Cernusak, A. I. Boldyrev, L. S. Wang, *J. Chem. Phys.* **2013**, *139*, 104312.

[25] Z. Yang, S. J. Xiong, *J. Chem. Phys.* **2008**, *128*, 184310.

[26] a) K. A. Nguyen, K. Lammertsma, *J. Phys. Chem. A* **1998**, *102*, 1608 – 1614; b) Y. Li, Y. J. Liu, D. Wu, Z. R. Li, *Phys. Chem. Chem. Phys.* **2009**, *11*, 5703 – 5710.

[27] W. Z. Yao, J. B. Yao, X. B. Li, S. D. Li, *Acta. Phys.-Chim. Sin.* **2013**, *29*, 1219 – 1224.

[28] H. J. Zhai, L. S. Wang, D. Y. Zubarev, A. I. Boldyrev, *J. Phys. Chem. A* **2006**, *110*, 1689 – 1693.

[29] A. N. Alexandrova, E. Koyle, A. I. Boldyrev, *J. Mol. Model.* **2006**, *12*, 569 – 576.

[30] W. L. Li, C. Romanescu, T. Jian, L. S. Wang, *J. Am. Chem. Soc.* **2012**, *134*, 13228 – 13231.

[31] L. Xie, W. L. Li, C. Romanescu, X. Huang, L. S. Wang, *J. Chem. Phys.* **2013**, *138*, 034308.

[32] a) A. D. Becke, *Phys. Rev. A* **1988**, *38*, 3098 – 3100; b) J. P. Perdew, *Phys. Rev. B* **1986**, *33*, 8822 – 8824.

[33] J. M. L. Martin, A. Sundermann, *J. Chem. Phys.* **2001**, *114*, 3408 – 3420.

[34] a) T. H. Dunning, *J. Chem. Phys.* **1989**, *90*, 1007 – 1023; b) R. A. Kendall, T. H. Dunning, R. J. Harrison, *J. Chem. Phys.* **1992**, *96*, 6796 – 6806.

[35] a) H. J. Zhai, S. Li, D. A. Dixon, L. S. Wang, *J. Am. Chem. Soc.* **2008**, *130*, 5167 – 5177; b) S. Li, H. J. Zhai, L. S. Wang, D. A. Dixon, *J. Phys. Chem. A* **2012**, *116*, 5256 – 5271; c) W. L. Li, C. Romanescu, Z. A. Piazza, L. S. Wang, *Phys. Chem. Chem. Phys.* **2012**, *14*, 13663 – 13669.

[36] a) G. D. Purvis, R. J. Bartlett, *J. Chem. Phys.* **1982**, *76*, 1910 – 1918; b) G. E. Scuseria, C. L. Janssen, H. F. Schaefer, *J. Chem. Phys.* **1988**, *89*, 7382 – 7387; c) K. Raghavachari, G. W. Trucks, J. A. Pople, M. Head-Gordon, *Chem. Phys. Lett.* **1989**, *157*, 479 – 483; d) J. D. Watts, J. Gauss, R. J. Bartlett, *J. Chem. Phys.* **1993**, *98*, 8718 – 8733; e) R. J. Bartlett, M. Musial, *Rev. Mod. Phys.* **2007**, *79*, 291 – 352.

[37] a) S. K. Nayak, B. K. Rao, P. Jena, X. Li, L. S. Wang, *Chem. Phys. Lett.* **1999**, *301*, 379 – 384; b) A. N. Alexandrova, A. I. Boldyrev, H. J. Zhai, L. S. Wang, *J. Phys. Chem. A* **2004**, *108*, 3509 – 3517.

[38] D. Y. Zubarev, A. I. Boldyrev, *Phys. Chem. Chem. Phys.* **2008**, *10*, 5207 – 5217.

[39] L. S. Wang, H. S. Cheng, J. W. Fan, *J. Chem. Phys.* **1995**, *102*, 9480 – 9493.

[40] a) J. Akola, M. Manninen, H. Hakkinen, U. Landman, X. Li, L. S. Wang, *Phys. Rev. B* **1999**, *60*, 11297 – 11300; b) W. Huang, L. S. Wang, *Phys. Rev. Lett.* **2009**, *102*, 153401.

[41] a) D. Andrae, U. Haussermann, M. Dolg, H. Stoll, H. Preuss, *Theor. Chim. Acta.* **1990**, *77*, 123 – 141; b) W. Küchle, M. Dolg, H. Stoll, H. Preuss, Pseudopotentials of the Stuttgart/Dresden Group (revision: August 11, 1998), **1998** (http://www.theochem.uni-stuttgart.de/pseudopotentials).

[42] M. J. Frisch, G. W. Trucks, H. B. Schlegel, Revision D.01 ed., Gaussian, Inc., **2004**.

[43] H. J. Werner, P. J. Knowles, G. Knizia, F. R. Manby, M. Schütz, et al., MOLPRO, version 2010.1, a package of ab initio programs, **2010**, http://www.molpro.net.

[44] U. Varetto, Molekel 5.4.0.8, Swiss National Supercomputing Centre, Manno, Switzerland, **2009**.

[45] R. Dennington, T. Keith, J. Millam, GaussView, Version 4.1, Semichem, Inc., Shawnee Mission, KS, **2007**.

[46] a) S. J. A. van Gisbergen, J. G. Snijders, E. J. Baerends, *Comput. Phys. Commun.* **1999**, *118*, 119 – 138; b) X. Li, B. Kiran, J. Li, H. J. Zhai, L. S. Wang, *Angew. Chem.* **2002**, *114*, 4980 – 4983; *Angew. Chem. Int. Ed.* **2002**, *41*, 4786 – 4789; c) J. Li, X. Li, H. J. Zhai, L. S. Wang, *Science* **2003**, *299*, 864 – 867; d) X. Huang, H. J. Zhai, J. Li, L. S. Wang, *J. Phys. Chem. A* **2006**, *110*, 85 – 92.

